5-2016

Expression, Purification, Enzymatic and Inhibition Profile of Brugia malayi Dihydrofolate Reductase

Romy Perez-Abraham
Montclair State University

MONTCLAIR STATE UNIVERSITY

/ Expression, Purification, Enzymatic and Inhibition Profile of *Brugia malayi*

Dihydrofolate Reductase /

by

Romy Perez-Abraham

A Master's Thesis Submitted to the Faculty of

Montclair State University

In Partial Fulfillment of the Requirements

For the Degree of

Master of Science Chemistry – concentration in Biochemistry

May 2016

College of Science and Mathematics Thesis Committee:

Department Chemistry/Biochemistry [redacted]

Thesis Sponsor: Dr. Nina Goodey

[redacted]

Committee Member: Dr. Ueli Gubler

[redacted]

Committee Member Dr. John Siekierka

Abstract

Dihydrofolate reductase (DHFR) is an essential enzyme that plays an important role in the production of cofactors that are required in deoxyribonucleic acid (DNA) synthesis. The literature suggests that DHFR is a potential drug target for the elimination of the parasitic worm, *B. malayi*. *B. malayi* is one of the causative parasites of lymphatic filariasis, a globally neglected tropical disease. In this study, we expressed and purified *B. malayi* DHFR. Expression was carried out in *E. coli* with a His6-tagged construct, and purification was achieved through affinity chromatography using a special strain of *E. coli* cells called "LOBSTR." The resulting purified and active enzyme was used for steady-state kinetics characterization and inhibition studies. The catalytic activity, k_{cat}, was found to be 1.4 ± 0.1s^{-1}, the Michaelis Menten constant, K_M, 14.7 ± 3.6μM for dihydrofolate, and the equilibrium dissociation constant, K_D, 22 ±0.01μM. *B. malayi* DHFR was compared to 13 other DHFR homologs in terms of ligand specificity determining residues; *L. major, T. cruzi, T. bruci,* and *T. gondii* exhibited the highest homology. Known inhibitors of these DHFR homologs were assayed with *B. malayi* DHFR and an inhibition profile was created for the enzyme. IC_{50} values were determined to be 0.0036 ± 0.0008 μM for methotrexate, 109 ± 34 μM for pyrimethamine, 32 ± 22 μM for trimethoprim, 771 ± 44 μM for cycloguanil, >20,000 μM for 2,4-diaminopyrimidine, and 154 ± 46 μM for 2,4-diaminoquinazoline. These results provide the basis for the development of more potent and less toxic compounds that can inhibit *B. malayi* DHFR and help cure lymphatic filariasis.

EXPRESSION, PURIFICATION, ENZYMATIC AND INHIBITION PROFILE OF *BRUGIA MALAYI* DIHYDROFOLATE REDUCATASE

A THESIS

Submitted in partial fulfillment of the requirements

For the degree of Masters of Science Chemistry – concentration in Biochemistry

by

ROMY PEREZ-ABRAHAM

Montclair State University, NJ

Montclair, NJ

2016

Acknowledgements

I would like to thank my thesis sponsor and career advisor, Dr. Nina Goodey, for all her support and guidance, and for allowing me to be part of her lab to complete this wonderful project. Also, Dr. Ueli Gubler for his guidance in my learning process and his indispensable input throughout the course of this project.

I would like to give a special thanks to graduate student Karla Sanchez who worked very hard for two years to get this project started and first cloned and expressed *B. malayi* DHFR. Karla also taught me all the necessary skills to work in a lab.

In addition, I would like to thank the department of Chemistry/Biochemistry in the School of Science and Mathematics and the Margaret and Herman Sokol Institute for Pharmaceutical Life Sciences at Montclair State University for providing the resources and work space to carry out this research. Special thanks to Dr. John Siekierka and lab members for allowing us to work in their same lab space and for sharing many of their instruments/supplies.

Finally, I would like to thank my mother, Sonia Abraham, for her unconditional love and support throughout my graduate studies, my father, Juan Perez, for always believing in me, and the rest of my family and friends who were always there along the way.

Table of Contents

Page Number

1. Introduction

1.1 Disease background

Lymphatic filariasis, also known as elephantiasis, is a neglected disease that affects more than 120 million people in 80 countries worldwide. This parasitic disease is caused by the nematodes *W. bancrofti, B. timori,* and *B. malayi*; the latter is the focus of this research. The disease is transmitted by mosquitos that carry the infective stage larvae. Once the larvae enter the blood of a human host, they develop into adult female and male worms located in the lymphatic system. The lymphatic system damage caused by this parasite is especially detrimental to the infected population because the lymphatic system is an essential component of the immune system.[19]

Figure 1 & 2. *B. malayi* in a blood smear.

Lymphatic filariasis is associated with poverty; there is an ongoing need for more potent and economic drugs for the elimination of this disease. In 1997 the World Health Organization declared the disease as "eradicable" and in 2000 a program started with the purpose to eliminate the disease. This program has as its goals to stop transmission and control morbidity by administrating the combination of two sets of drugs,

diethylcarbamazine citrate (DEC) and albendazole, or ivermectin and albendazole once a year for at least 5 years in areas prone to the occurrence of the disease. Two pharmaceutical companies, GlaxoSmithKline and Merck & Co. Inc. pledge to provide these drugs at no cost for as long as it takes to reach the set goals. Out of the 72 countries targeted by the program, so far only two countries, the Republic of Korea and China, have declared elephantiasis as no longer a threat to their population. In general, the progress seems to be going rather slow, a fact that can be attributed mostly to the prevalent ongoing need to understand the epidemiology of elimination of lymphatic filariasis.

1.2 Target overview

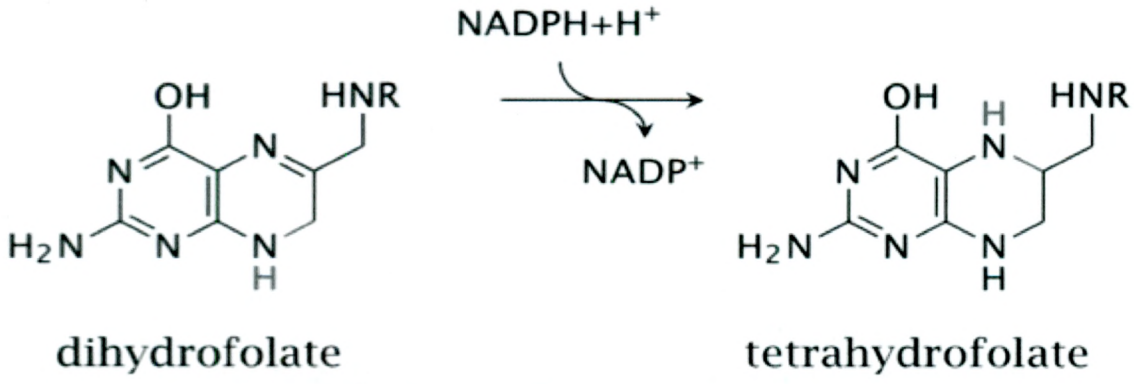

Figure 3. Dihydrofolate is reduced to tetrahydrofolate by the enzyme dihydrofolate reductase (DHFR). DHFR catalyzes the transfer of a hydride from the cofactor NADPH, which in turns gets protonated.

Dihydrofolate reductase (DHFR) is a monomeric enzyme of about 20KDa that has been evolutionarily well conserved. It catalyzes the reaction from dihydrofolate to tetrahydrofolate in the presence of NADPH. Tetrahydrofolate is a precursor of cofactors

necessary for the synthesis of purines, pyrimidines, and many amino acids, which are necessary for cell proliferation and growth.

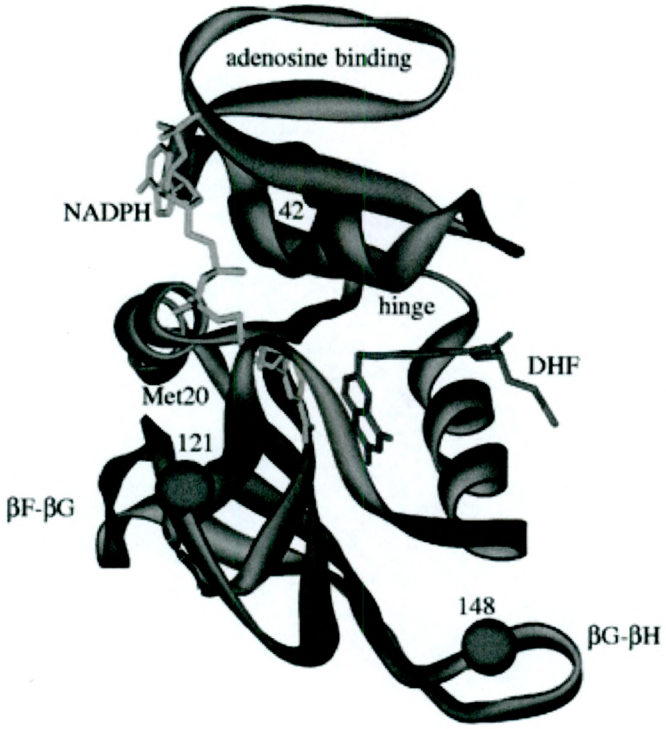

Figure 4. 3D structure of *E. coli* DHFR. NADPH is shown in green and DHF is shown in magenta.

DHFR is a therapeutic target for infectious diseases.[15] Antifolates are a specific group of compounds that inhibit DHFR; the group includes anticancer, antibacterial and antimalarial drugs. DHFR inhibition by these antifolate compounds is mediated through the disruption of DNA biosynthesis and it is the basis of chemotherapeutic action.[7] The evaluation of synthetic antifolate agents, biguanide and dihydrotriazine, along with the drugs pyrimethamine and trimethoprim, has demonstrated that DHFR inhibitors could be promising molecules for the treatment of *B. malayi*.[2] Furthermore, the evaluation of 12 diverse antifolate compounds with 2,4-diaminopyrimidine and 2,4-diamino-*s*-triazine

structural features against *B. malayi* proves that DHFR inhibitors are indeed novel drug candidates against lymphatic filariasis.[16] However, these studies were done on *B. malayi*, not on the target; the purified *Bm*DHFR. Encouragement came from these findings to purify *Bm*DHFR and prove that the target can be inhibited with antifolate compounds, as predicted.

1.3 Project goals

1.3.1 Previous work (by Karla Sanchez)

The first goal of this project was to express and purify *B. malayi* DHFR for the first time. Before I joined this project, graduate student Karla Sanchez obtained the amino acid sequence of *Bm*DHFR from UniProt (A8QGA9) and engineered a His6-tag at the N-terminus. The purpose of the His6-tag is to enable the capture of the protein by nickel or cobalt ions on the specific resin used for purification.[1] The designed DNA-sequence was then codon optimized for expression in *E. coli* (Genewiz) and the resulting *Bm*DHFR DNA fragment was subcloned into the pET25b expression vector. At this point the project ran into some difficulties when *Bm*DHFR did not exhibit any catalytic activity. Dr. Goodey, Dr. Gubler, and Karla worked hard to fix this issue, and they realized that the problem came from the amino acid sequence of the enzyme. There are two different *Bm*DHFR sequences on UniProt, one of them (A8QGA9) was entered on August 2014 and was missing 13 amino acids (residues 113-125) essential for the folding of the protein; which will be referred to as the loop mutant or $\Delta_{113\text{-}125}$*Bm*DHFR from hereon. After the right sequence was obtained from UnitProt (A8QBG1, entered on March 2015), the same process previously explained was carried out on the full sequence and *Bm*DHFR exhibited catalytic activity.

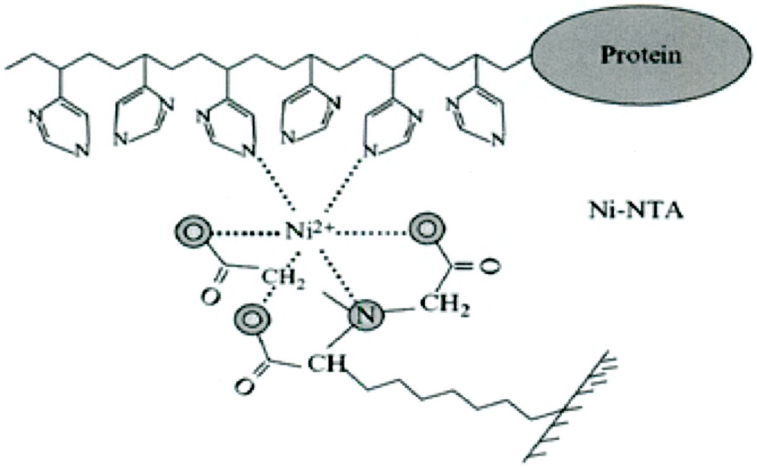

Figure 5. Ni-NTA resin interacting with polyhistidine tag.

1.3.2 My goals

Once I joined this project, the first challenge was to purify *B. malayi* DHFR, which had been expressed in BL21 (DE3) *E. coli* cells. The subsequent affinity chromatography purification yielded impure protein (<95%). It was speculated that the impurity most likely represented (a) contaminating histidine-rich *E. coli* protein(s) when using Ni-NTA affinity chromatography. Dr. Ueli Gubler suggested to introduce our pET25n-*Bm*DHFR plasmid into a recently described special *E. coli* expression strain, BL21 (DE3) derivative, called "LOBSTR" (low background strain). The LOBSTR strain is specifically engineered to eliminate the most abundant contaminants caused by His-mediated purification.[1] The approach works by lowering the background contamination due to ArnA (74 KDa) and SlyD (21 KDa), bifunctional enzymes involved in the modification of lipid A phosphates with aminoarabinose and a peptidyl-prolyl cis/trans-isomerase, respectively.[1] When recombinant protein expression is low, the protein starts competing with endogeneous ArnA and SlyD for binding to the Ni or Co resin, leading to the co-purification of ArnA and SlyD as impurities. The LOBSTR strain genomically modifies ArnA and SlyD by mutagenizing them to change the surface-expose His to Ser.

These modifications reduce the Ni and Co binding affinity of the unwanted host proteins.[1]

Kinetic characterization and enzyme inhibition studies followed the expression and purification of *Bm*DHFR. Kinetic parameters like K_M and k_{cat} serve as a comparison between different DHFRs from different organisms. The dissociation constant K_D serves as a comparison between the loop mutant and the wildtype in terms of the binding of the cofactor NADPH and the consequent folding of the protein. *Bm*DHFR is expected to bind with a greater affinity than $\Delta_{113\text{-}125}$*Bm*DHFR.

In order to complete an inhibition profile for the enzyme, it was necessary to make predictions of antifolate compounds that could potentially inhibit *Bm*DHFR. A novel phylogenetics-based method for predicting residues involved in inhibitor specificity in the DHFR family identified eighteen amino acid positions in thirteen DHFR homologs that are involved in ligand specificity (inhibitor binding).[5] With this information at hand, and by extensive alignments of the 13 DHFR homologs with *B. malayi* DHFR, the 18 amino acid positions predicted to be involved in inhibitor specificity were determined in the *Bm*DHFR sequence. The DHFR homologs with the highest percentage identity to the 18 amino acid residues in *Bm*DHFR were *L. major, T. cruzi, T. gondii, and T. bruci*. Known DHFR inhibitors of these organisms were predicted to also inhibit our enzyme and were obtained to generate an inhibition profile for *B. malayi* DHFR.

2. Methods and Materials

2.1. BmDHFR expression

BL21(DE3) or LOBSTR (Kerafast) cells were transformed with isolated pET25b-*Bm*DHFR DNA and expression of *Bm*DHFR was explored at room temperature and 30 °C. BL21(DE3) and LOBSTR transformants were grown in LB/amp (100ug/ml ampicillin) to an OD_{600} ~0.6 at 37 °C. Cultures were allowed to reach the desired expression temperatures and expression was induced with 0.3 mM IPTG. Cells were harvested after 5 hours and overnight. To extract soluble protein, cells were harvested by centrifugation at 5,000 rpm for 30 min, resuspended in ~15 mL of Equilibration Buffer (20 mM sodium phosphate, 300 mM NaCl (PBS), 10 mM imidazole, pH 7.4) and lysed by sonication for 4 min (output: 5, duty cycle: 10, W-225 Heat Systems Ultrasonics sonicator with microtip). Cell debris and soluble protein extract were separated by centrifugation at 5,000 rpm for 30 minutes (Beckman Coulter Avanti J-26S XP centrifuge with JA-10 rotor).

2.2. Purification of BmDHFR

Soluble cell lysate was loaded onto HisPur™ Ni-NTA Resin (Thermo Scientific) equilibrated in a gravity-flow column with Equilibration Buffer (20 mM sodium phosphate, 300 mM NaCl (PBS), 10 mM imidazole, pH 7.4). The resin was washed with Wash Buffer (PBS, 25 mM imidazole, pH 7.4) and *Bm*DHFR was eluted with Elution Buffer (PBS, 250 mM imidazole, pH 7.4). Wash and elution fractions were monitored for protein content by a microtiter-plate based Bradford assay.

2.3. BmDHFR activity assay

*Bm*DHFR activity was determined with saturating concentrations of NADPH and DHF (100 μM each) by measuring the change in absorbance at 340 nm. The differential extinction coefficient value of 13.2 $mM^{-1}cm^{-1}$ (for the combination of conversion of NADPH to NADP+ and DHF to THF) was used to convert the change in absorbance over time to an initial velocity. In a typical experiment, (reaction volume of 200 μl) *Bm*DHFR (45 to 85 nM) was incubated with NADPH (100 μM) for 2-3 min, adding DHF to a final concentration of 100 μM, and recording the absorbance at 340 nm for 3 minutes. All experiments were carried out in MTEN buffer (50 mM 2-morpholinoethane sulphonic acid (MES), 25 mM Tris, 25 mM ethanolamine, and 100 mM NaCl). The assays were completed in triplicate at 25 °C in a SpectraMax M3 microplate reader. The optimum pH for the DHFR reaction was determined by comparing the rate of change in absorbance at pH values ranging from 4 to 10 in one unit increments. Turnover number (k_{cat}) was calculated using the formula $k_{cat} = \frac{V_{max}}{[E]}$ at pH 6.00.

2.4. Determination of the Michaelis-Menten constant (K_M)

The affinity of *Bm*DHFR for its substrate DHF was determined by measuring the enzyme activity as a function of increasing concentrations of DHF. The concentration of DHF in the well ranged from 0.13 to 100 μM; dilutions were made in MTEN pH 6.0. NADPH (100 μM) and 46 nM enzyme were incubated for 2-3 min, DHF was added to initiate the reaction, and absorbance was recorded at 340 nm. As above, all experiments were completed at 25 °C in MTEN at pH 6.0 in a reaction volume of 200 μl. Initial

velocity was plotted as a function of DHF concentration using Kaleidagraph and the data was fitted to the Michaelis-Menten equation. Assays were completed in triplicate.

2.5. Prediction of BmDHFR Inhibitors

Previous research predicted that 18 amino acid positions in 13 selected DHFR homologs would play a role in enzyme in inhibition.[5] The 18 residues were identified in *Bm*DHFR by aligning its entire sequence with the sequences of the 13 homologues in MEGA software. The unwanted amino acid residues were deleted from each of the 14 sequences using MEGA software, leaving the sequences with only the desired 18 amino acid positions. An individual alignment was done between the 18 residues of *Bm* and each of the 13 homologs; the percent alignment identity was recorded. A literature search was conducted with the top 4 homologous DHFR proteins having the highest percent identity to Bm DHFR. The drugs that inhibit those 4 homologs were predicted to also inhibit *Bm* DHFR and were subsequently used for inhibition studies.

2.6. Effects of DMSO concentration on *Bm*DHFR activity.

Stock solutions of predicted *Bm*DHFR inhibitors were prepared in DMSO. Control experiments with DMSO were conducted to confirm that DMSO at the relevant concentrations did not affect *Bm*DHFR activity. The assay was set up the same way, with concentrations of 100 μM and 46 nM for NADPH and *Bm*DHFR respectively.15 ul DMSO stocks resulting in concentrations ranging from 18% to 75% were included in the assay as replacement for the inhibitors. The final concentration of DMSO in the inhibitions assays was always below 3 % in all experiments meaning the activity of

*Bm*DHFR was not be affected by the inclusion of DMSO; DMSO did not inhibit *Bm*DHFR.

2.7. Inhibition Studies

Methotrexate (MTX, Sigma M9929), pyrimethamine (PMT, Fluka 46706), 2,4-diaminopyrimidine (Sigma 468231), 2,4-diaminoquinazoline (Sigma CDS001152), trimethoprim (TMP, MP Biomedicals 0910013), and cycloguanil (CYC, Cayman 16861) were evaluated as inhibitors of *Bm*DHFR catalytic activity. Stock solutions were prepared in DMSO and dilutions of all stock solutions were made in MTEN pH 6.0. *Bm*DHFR activity was measured as described above, with varying concentrations of inhibitor added. NADPH (100 μM) and *Bm*DHFR (46 nM) in a total volume of 200 μl were incubated with 15 μl inhibitor (varying concentrations in different wells) for 2-3 minutes before the reaction was initiated by adding DHF (final concentration 20 μM, final reaction volume 200 ul). Percent activity for each inhibitor concentration was obtained by dividing the rate from the inhibition experiment by the rate of the control experiment where no inhibitor was added. Dose response curves were generated in Kaleidagraph. Data was fitted to the Hill equation.

$$\%\ \text{response} = \text{min response} + (\text{max response} - \text{min response})/\left(1 + \frac{IC_{50}}{[\text{inhibitor}]}\right)^{-1}$$

with n = -1. IC_{50} values for each inhibitor were calculated. All assays were completed in triplicate.

2.8. Determination of equilibrium dissociation constant

The thermodynamic dissociation constant (K_D) for the binding of NADPH to *Bm*DHFR and $\Delta_{113\text{-}125}$*Bm*DHFR was determined by monitoring the tryptophan fluorescence (ex. 290 nm/em. 340 nm) as NADPH was added to 228 nM enzyme (wildtype) and 172 nM ($\Delta_{113\text{-}125}$*Bm*DHFR) in MTEN, pH 6.0 at room temperature. The NADPH concentration ranged from 0 to 1.4 mM.

3. Results and Discussion

3.1. Expression and purification of recombinant *Bm*DHFR

Based on the UniProt database amino acid sequence A8G6A9, the DNA sequence coding for *Bm*DHFR was designed to incorporate an N-terminal His6-tag. The sequence was codon optimized for expression in *E. coli* (Genewiz) and the resulting *Bm*DHFR DNA fragment was subcloned into the pET25b expression vector. This pET25b-*Bm*DHFR plasmid was introduced into the BL21(DE3) derivative, "LOBSTR".[1] Several small-scale expression studies revealed that soluble *Bm*DHFR protein expression could be obtained by induction with 0.3 mM IPTG at room temperature for 24 hours.

For larger scale purification, soluble protein was derived from an induced 250 mL culture by sonication and centrifugation, and the resulting supernatant was applied to a standard Ni-NTA affinity column. Purification of the soluble, recombinant *Bm*DHFR can be completed through this single step if expression is performed in the "LOBSTR" expression strain. SDS-PAGE analysis of the eluate showed that the enzyme had the expected size of approximately 22 kDa, consistent with the predicted molecular weight of 22.086 kDa calculated from the DNA sequence (Figure 7). Expression and purification

via this method yielded ~1.8 mg purified *Bm*DHFR/L of induced culture. Concentration of *Bm*DHFR was 46 nM. However, when expression was carried out in the standard BL21(DE3) strain, followed by Ni-NTA chromatography of soluble protein, a ~66 kDa contaminant remained in the eluted protein fractions (Figure 6).

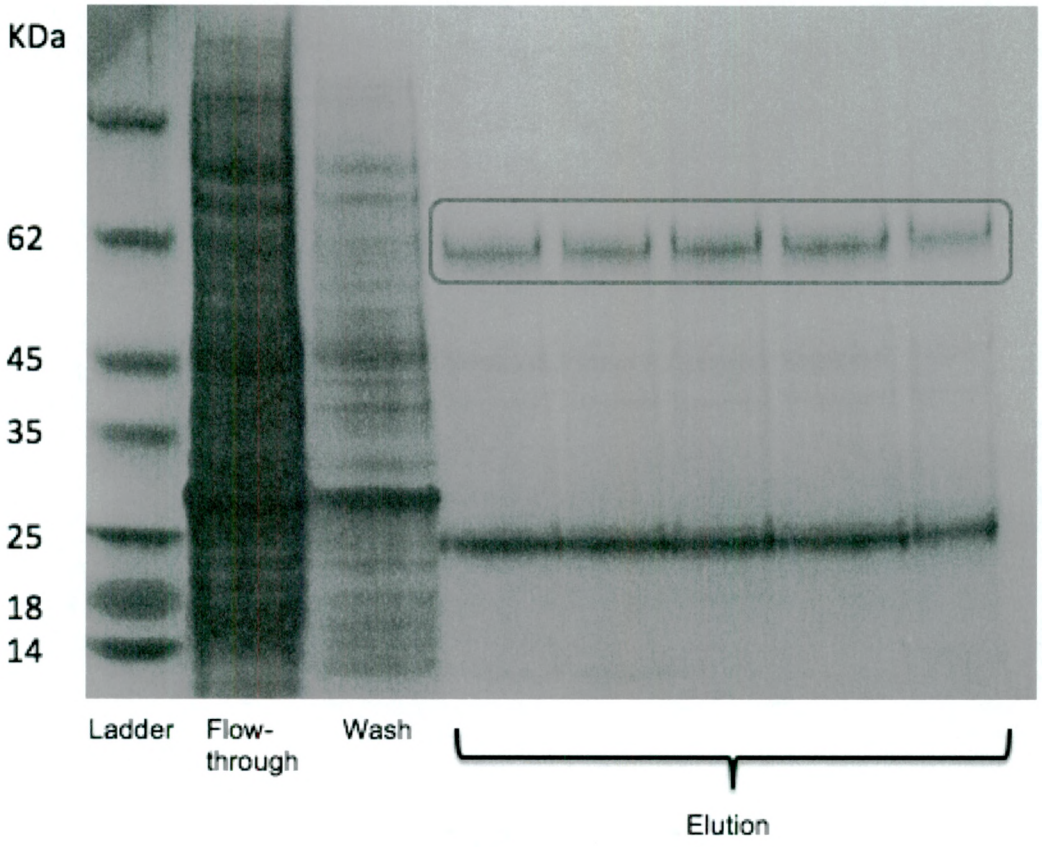

Figure 6. SDS-PAGE analysis of *Bm*DHFR expression and purification in the BL21 (DE3) *E. coli* expression strain. The Ni-NTA column one step purification resulted in <95% pure protein due to the histidine-rich host proteins that were co-purified. Lane 1. Ladder (Fisher Bioreagents EZ-Run Protein Standard BP3600); Lane 2. Flow-through; Lane 3. Wash; Lanes 4-8. Elution fractions from the Ni-NTA column.

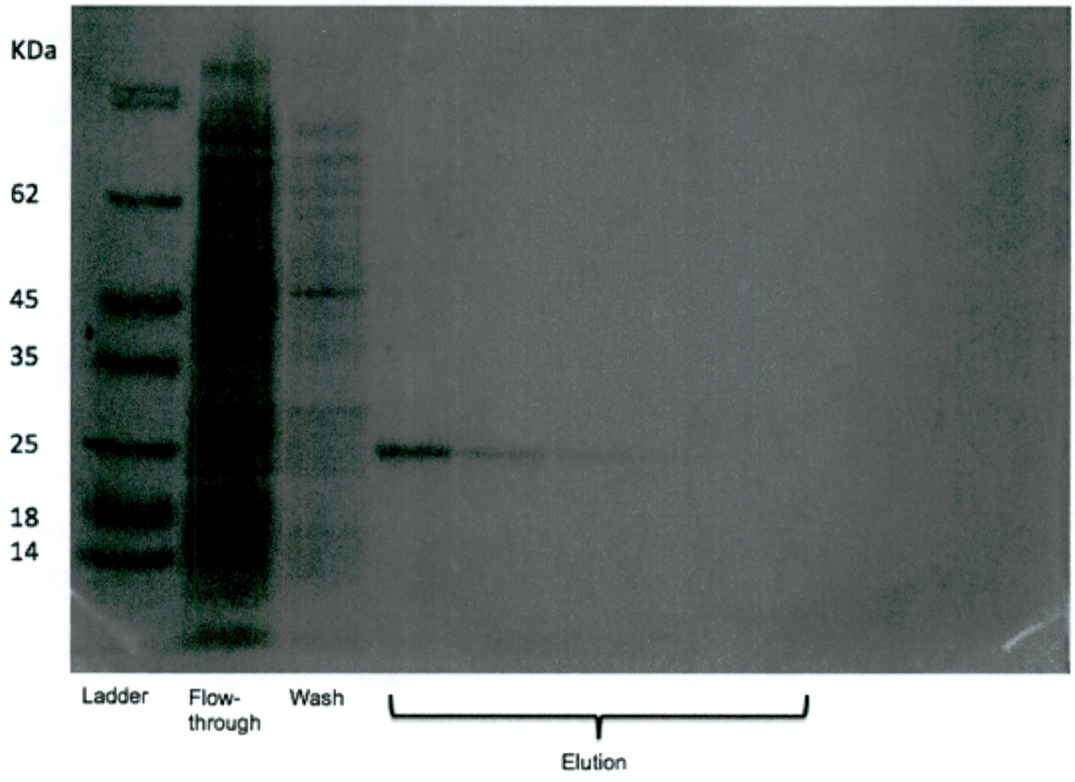

Figure 7. SDS-PAGE analysis of *Bm*DHFR expression and purification in the LOBSTR *E. coli* expression strain. The Ni-NTA column one step purification resulted in >95 % pure protein. Lane 1. Ladder (Fisher Bioreagents EZ-Run Protein Standard BP3600); Lane 2. Flow-through; Lane 3. Wash; Lanes 4-7. Four separate elution (1 mL each) fractions from the Ni-NTA column.

3.2. BmDHFR activity assay

After the expression and purification of *Bm*DHFR, the next step was the make sure the enzyme had catalytic activity. This was tested on a 96-well plate reader using different concentrations of enzyme until there was an evident decrease in absorbance, i.e.

a slope in the plot of absorbance vs. time at a wavelength of 340nm. The concentrations of DHF and NADPH were 100 μM each and *Bm*DHFR was 46 nM.

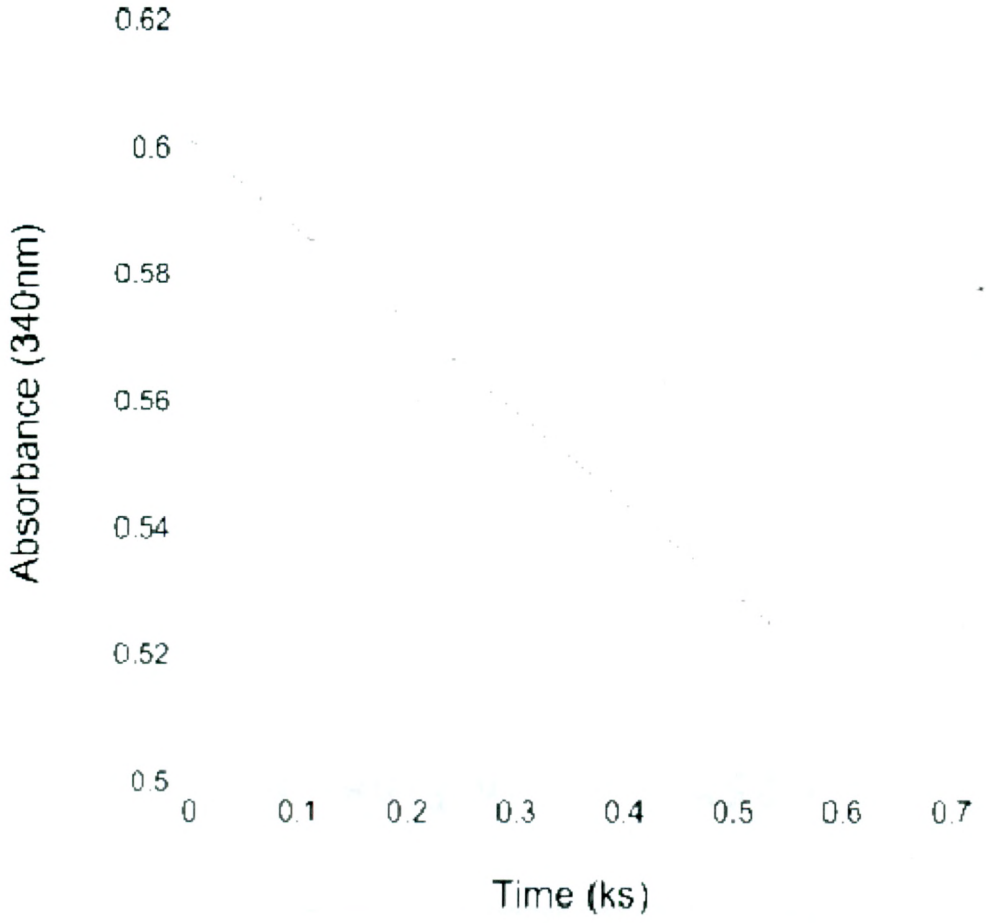

Figure 8. *Bm*DHFR catalytic activity with saturating concentrations of NADPH and DHF (100 μM each) and concentration of *Bm*DHFR of 46 nM. Change in absorbance was measure at 340nm over 10 minutes. The differential extinction coefficient value of 13.2 $mM^{-1}cm^{-1}$ (for the combination of conversion of NADPH to NADP+ and DHF to THF) was used to convert the change in absorbance over time to an initial velocity.

3.3. Kinetic Characterization of *Bm*DHFR

The dependence of the catalytic activity on pH was explored; catalytic activity was found to be highest at pH ~ 6.0 (Figure 10). The k_{cat} value for *Bm*DHFR was determined at pH 6.0 to be 1.4 ± 0.1s^{-1} (Figure 9) and the K_M for DHF 14.7 ± 3.6 μM (Figure 11).

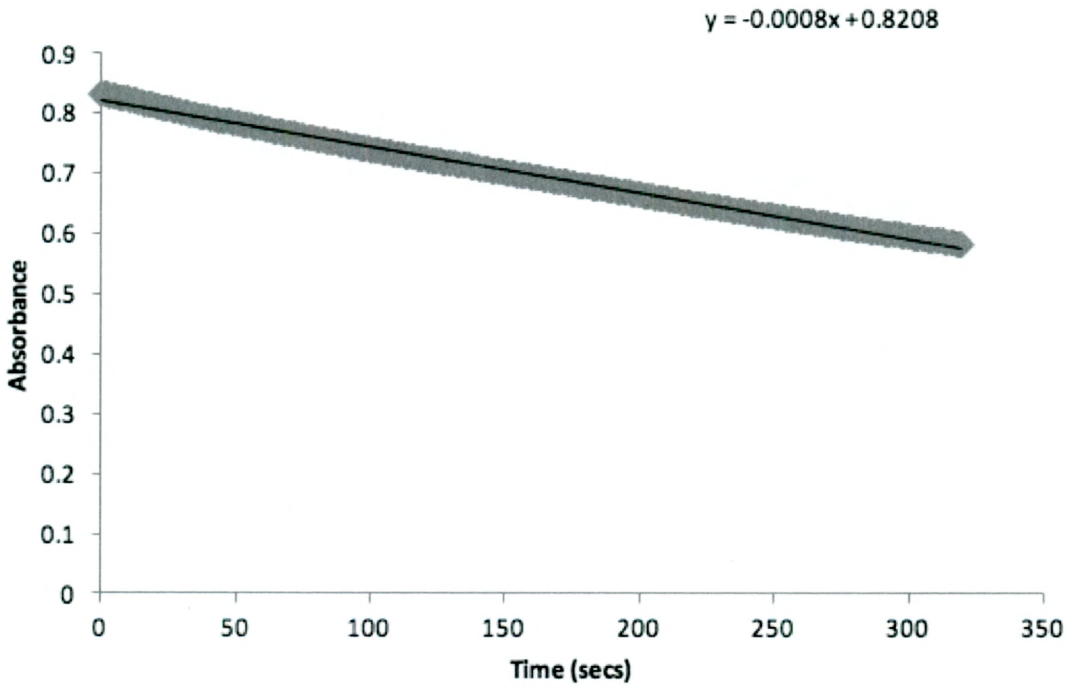

Figure 9. A representative graph of three trials of k_{cat} measurements at a wavelength of 340nm. This experiment was carried out in a spectrophotometer using a 1 mL plastic cuvette as oppose to the other experiments that were conducted in a 96-well plate spectrophometer. The enzyme concentration in the assay was 78.6 nM. The average of the three individual trials gave a k_{cat} of 1.4 ± 0.1s^{-1}.

Sample of calculation of k_{cat}:

$$\frac{\Delta C}{time} = \frac{slope}{\varepsilon \times l} = \frac{0.0008}{(13.2 mM^{-1} cm^{-1})(1cm)(s)} = 0.0000606 mM s^{-1}$$

$$Kcat = \frac{0.0000606mMs^{-1}}{0.0000393mM} = 1.542s^{-1}$$

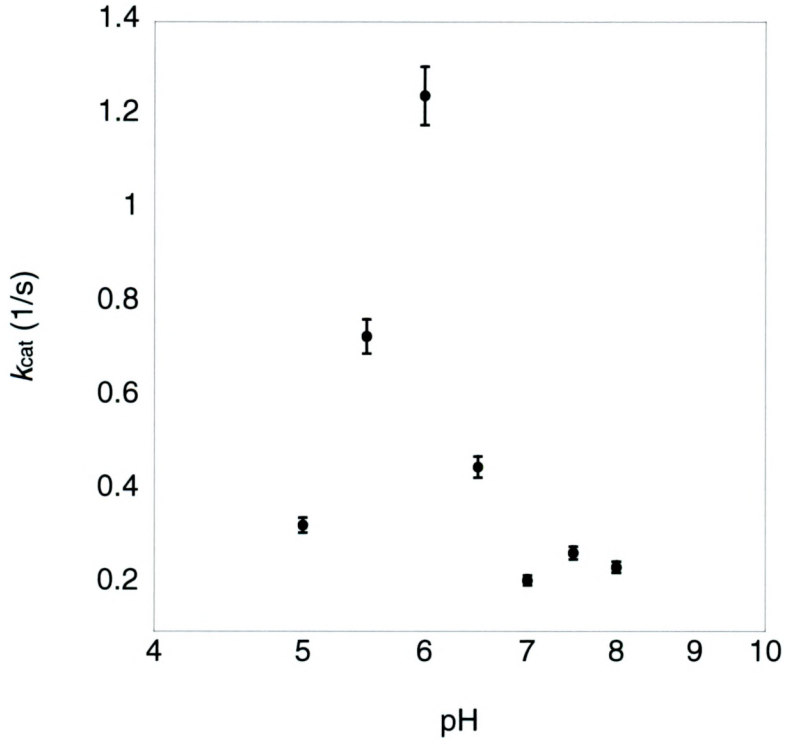

Figure 10. Dependence of catalytic activity of *Bm*DHFR on pH. Individual experiments were conducted in a 96-well plate at room temperature with 100 μM NAPDH, 100 μM DHF and 46 nM *Bm*DHFR. The buffer used was MTEN (1250mM MES, 125mM Tris, 125mM ethanolamine, 500mM NaCl) with pH ranging from 5.5 to 12. The reported data is an average of duplicate measurements.

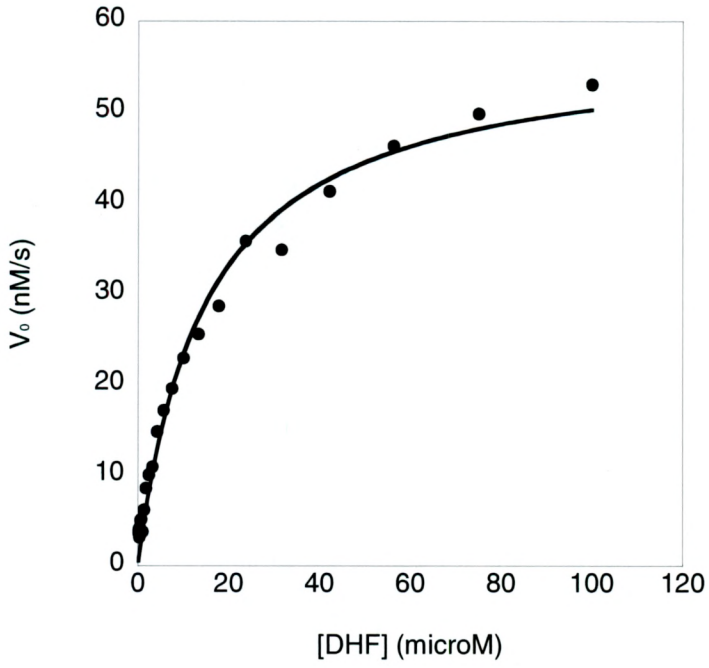

Figure 11. Steady-state kinetic analysis of *Bm*DHFR gives a K_M value for DHF of 14.7 ± 3.6 μM and a V_{max} value of 57 ± 14 $nM*s^{-1}$ (n=3). The data shown is representative for one out three experiments. Rate of change of absorbance at 340 nm was measured as a function of DHF concentration with 100 μM NADPH and 0.045 μM *Bm*DHFR at pH 6.0 at room temperature. Michaelis-Menten curves were generated in KaleidaGraph and report initial velocity ($mM*s^{-1}$) versus [DHF] (μM).

3.4. Prediction of inhibitor profile against BmDHFR using PAn Predictor

We used a variation of the previously published computational approach ("PAn Predictor") to predict antifolate compounds that might serve as effective inhibitors of *Bm*DHFR.[5] First, we aligned the 13 DHFR homolog sequences used originally to predict inhibitor specificity determinants in the DHFR family with *Bm*DHFR and identified the

18 residues in *Bm*DHFR corresponding to the 18 amino acid positions that are inhibitor specificity determinants in the DHFR family.[5] These positions in *Bm*DHFR are Val5, Gly12, Met27, Asn44, Ala45, Lys51, Phe60, Val84, Phe89 Leu95, Leu96, Gly133, Ala137, Val139, Phe140, Phe141 and Glu169 (Figure 12). The *Bm*DHFR residue corresponding to the putative catalytic acid (Asp 27) in *E. coli* DHFR is Glu26 (indicated by # in Figure 12). The requirement for the Glu26 to be in the protonated state may correspond with the sharp decrease in activity as the pH increases shown in Figure 10.

```
                *       *                  #*                  **
BmDHFR  ....MNLIVA VDGCGGIGRN GGMPW.FLPA EMARFAKLTT LTMDSGKKNA 45
HsDHFR  MVGSLNCIVA VSQNMGIGKN GDLPWPPLRN EFRYFQRMTT TSSVEGKQNL 50
EcDHFR  ...MISLIAA LAVDRVIGME NAMPW.NLPA DLAWFKRNTL .......NKP 39
                                           |
        *    *         *                          *           *
BmDHFR  VIMGRKVWES IPPKFRPLKN RFNVVLSRKI KEESNENVVV ARSFESAISL 95
HsDHFR  VIMGKKTWFS IPEKNRPLKG RINLVLSREL KEPPQGAHFL SRSLDDALKL 100
EcDHFR  VIMGRHTWES I...GRPXPG RKNIILSSQ. .PGTDDRVTW VKSVDEAIAA 84

        *                                              *   * ****
BmDHFR  LQDME...NI ETIWNIGGRE VYELGLNSPF LHQMYITRVE GDFLADVFFP 142
HsDHFR  TEQPELANKV DMVWIVGGSS VYKEAMNHPG HLKLFVTRIM QDFESDTFFP 160
EcDHFR  AG......DV PEIMVIGGGR VYEQFL..PK AQKLYLTHID AEVEGDTHFP 126

                                           *
BmDHFR  EVDYGRFI.K STES....EE MHEEKGIKYR YEIYTVKIDK VA 179
HsDHFR  EIDLEKYK.L LPEYPGVLSD VQEEKGIKYK FEVY....EK ND 187
EcDHFR  DYEPDDWESV FSEF....HD ADAQNSHSYS FEIL....ER R. 159
```

Figure 12. Alignment of *Bm*DHFR sequence with *H. sapiens* and *E. coli* DHFRs. The 18 amino acid positions that are predicted as inhibitor specificity determinants in the DHFR family are identified by bold letters. These 18 residues were identified in *H. sapiens* and *E. coli* DHFRs by previously published approach PAn Predictor, and in *Bm*DHFR by an alignment with the 13 DHFR homologs, including Hs and Ec.[5] The catalytic residue Asp27 is labeled on the *E. coli* sequence (#) and the corresponding Glu17 is labeled on

the *B. malayi* sequence (|). (Howell et al. 1986) The horizontal rectangle is showing the loop mutant on the *B. malayi* sequence.

We then determined the percentage identity between *Bm*DHFR and other DHFR sequences based on only these 18 specificity determining residues. This analysis showed that DHFR sequences from *L. major* and *T. cruzi* had the highest homologies (>70%) to *Bm*DHFR (Table 1).

Entry	Organism	Set 1	Set 2	Set 3
P07382	*Lm*	72.2%	72.2%	66.6%
Q27793	*Tc*	72.2%	61.1%	61.1%
Q27783	*Tb*	66.6%	55.5%	55.5%
Q07422	*Tg*	66.6%	55.5%	55.5%
P16184	*Pc*	61.1%	61.1%	55.5%
O02604	*Pv*	50.0%	50.0%	44.4%
P13922	*Pf*	50.0%	44.4%	44.4%
P00374	*Hs*	44.4%	50.0%	44.4%
Q920D2	*Rn*	44.4%	50.0%	44.4%
P9WNX1	*Mt*	16.6%	16.6%	11.1%
P0ABQ4	*Ec*	11.1%	22.2%	11.1%
O30463	*Ma*	11.1%	11.1%	11.1%
P00381	*Lc*	5.5%	16.6%	5.5%

Table 1. Highest to lowest percentage identity of 13 organisms to *Bm*DHFR. Sets 1, 2, and 3 consist of 15, 15, and 12 amino acid positions, respectively.[5] In every set, each DHFR homolog sequence was aligned with *Bm*DHFR and the percentage identity was determined. At the top of the list is the organism, *L. major* DHFR, which was the most similar to *Bm*DHFR based on the 18 specificity-determining residues. The inhibitors were

then selected based on this information and by doing a literature search of the drugs that inhibit the top 4 organisms with the highest percent identity to *Bm*DHFR.

A subsequent literature search and examination of BindingDB (Liu, T 2007) allowed us to identify a set of six known DHFR inhibitors that inhibit DHFRs with high homology to *Bm*DHFR in terms of the 18 residues studied. The IC_{50} values of these six compounds against *Bm*DHFR were determined.

Drugs	Inhibition Activity	DHFR homolog	IC50 (uM)	Ki (uM)	Ki reference article	IC50 reference article
Pyrimethamine	weak	*L. major*		0.25	Gilbert, 2002	
Trimethoprim	weak	*L. major*	~16.5	0.12	Gilbert, 2002	White, et al. 2004
Cycloguanil	weak	*L. major*	0.011	5.8uM	Gilbert, 2002	Basco, et al. 1994
Methotrexate	potent	*T. cruzi*	~0.0083	$3.8X10^{-5}$	Gilbert, 2002	White, et al. 2004
2,4-Diaminopyrimidine	potent	*L.major/T. gondii/T. cruzi*	0.2	0.0078	Pez, et al. 2003	Pez, et al. 2003
2,4-Diaminoquinazoline	potent	*L. major*	0.2	0.0070	Khabnadideh, et al. 2005	Khabnadideh, et al. 2005

Table 2. Known drugs that bind the DHFR homolog sequences with the highest percentage identity to *Bm*DHFR. The drugs exhibiting potent inhibition activity, low IC50's and Ki's were selected to be acquired for further studies.

3.5. Effects of DMSO concentration on *Bm*DHFR activity.

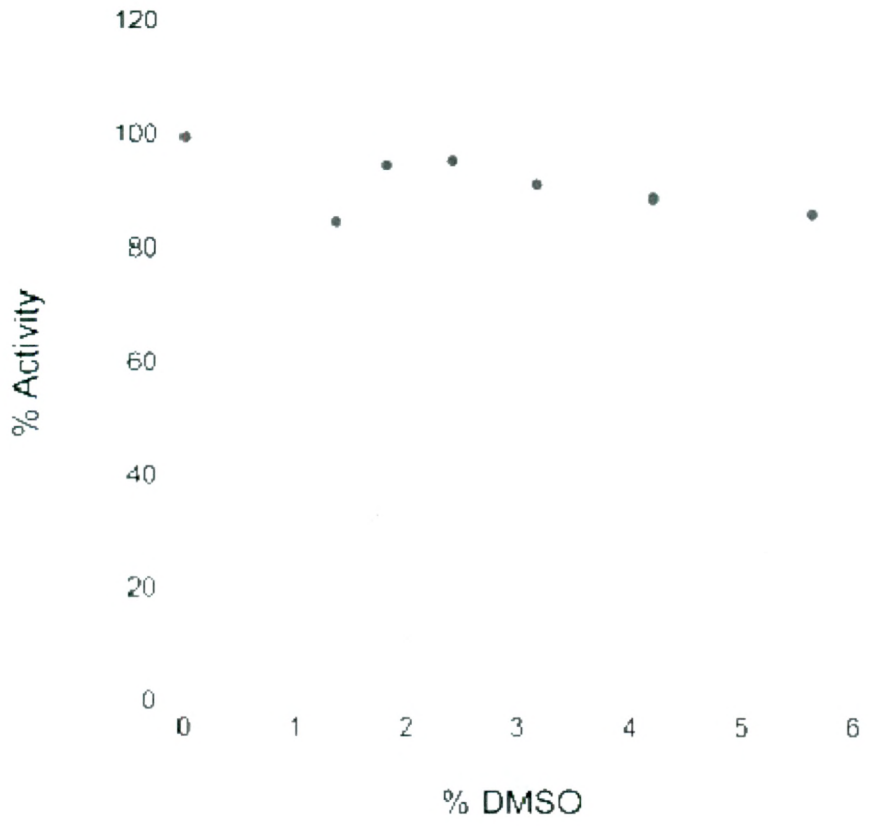

Figure 13. *Bm*DHFR activity at concentrations of DMSO ranging from 18% to 75% (stock) and 1.4% to 5.6% (in assay). Graph shows that the enzyme retained its catalytic activity when assayed in various concentrations of DMSO instead of the inhibitor, proving that DMSO does not alter the inhibition studies results. Individual experiments were conducted in a 96-well plate at room temperature with conditions in the well of 100 μM NAPDH, 100 μM DHF and 46 nM *Bm*DHFR. Percent activity was obtained by calculating the slope of the line (abs. at different conc. of DMSO vs. time) over the slope of the line (abs. with no DMSO vs. time) times 100%.

3.6. Inhibition by antifolate compounds

Determination of IC_{50} values of six antifolate compounds against recombinant *Bm*DHFR showed that methotrexate was the most potent inhibitor of the six compounds tested against *Bm*DHFR with an IC_{50} value of 4.0 ± 0.8 nM (Table 3). Pyrimethamine, trimethoprim, cycloguanil, and 2,4-diaminoquinazoline were found to inhibit *Bm*DHFR with IC_{50} values of 109 ± 34, 32 ± 22, 771± 44 and 154 ± 46 μM, respectively (Tables 4-7). The inhibitor 2,4-diaminopyrimidine did not inhibit *Bm*DHFR at concentrations below 20 mM.

3.6.1. Methotrexate

Inhibition curve, IC50 and K_I determination:

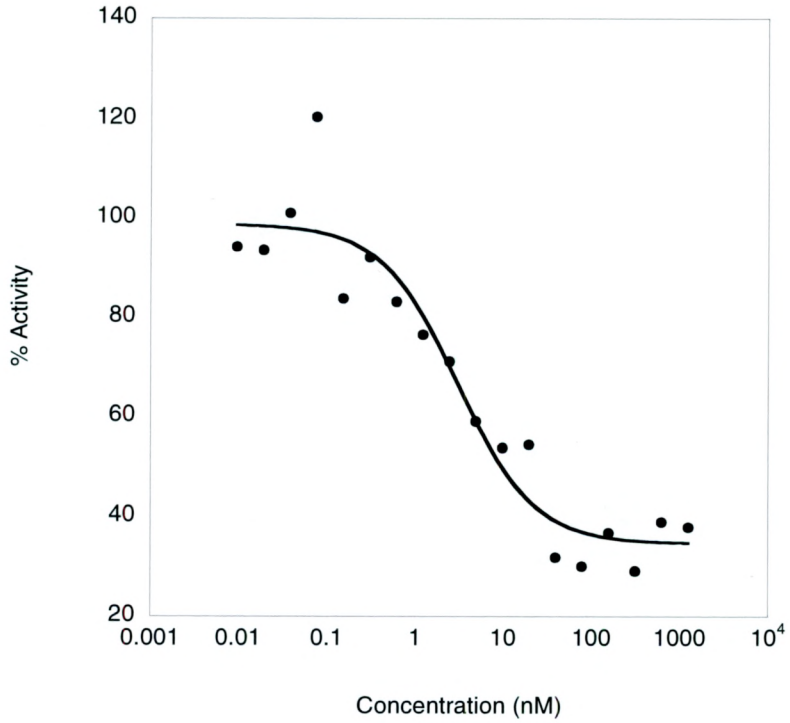

Figure 14. A representative graph of a *B. malayi* DHFR inhibition curve in the presence of the inhibitor Methotrexate. The average of three trials gave an IC50 of 0.0040 ± 0.0008μM. Individual experiments were conducted in a 96-well plate at room temperature with conditions in the well of 100 μM NAPDH, 100 μM DHF and 46 nM *Bm*DHFR. Percent activity in the y-axis was determined by dividing the slope of the abs. of methotrexate at different concentrations vs. time over the slope of the assay (abs. vs. time) with no inhibitor, and multiplying by 100%.

MTX	**IC50 (μM)**	**K_I (μM)**
Trial 1	0.0032998	0.001397898
Trial 2	0.0030152	0.001277333
Trial 3	0.0045142	0.001912356
Average	0.003609733	0.001529195
Std. dev.	0.000796112	0.000337258
Average ± Std. dev.	0.004 ± 0.0008	0.002 ± 0.0003

Table 3. IC50 and K_I from three trials of Methotrexate.

3.6.2. Pyrimethamine

Inhibition curve, IC50 and K_I determination:

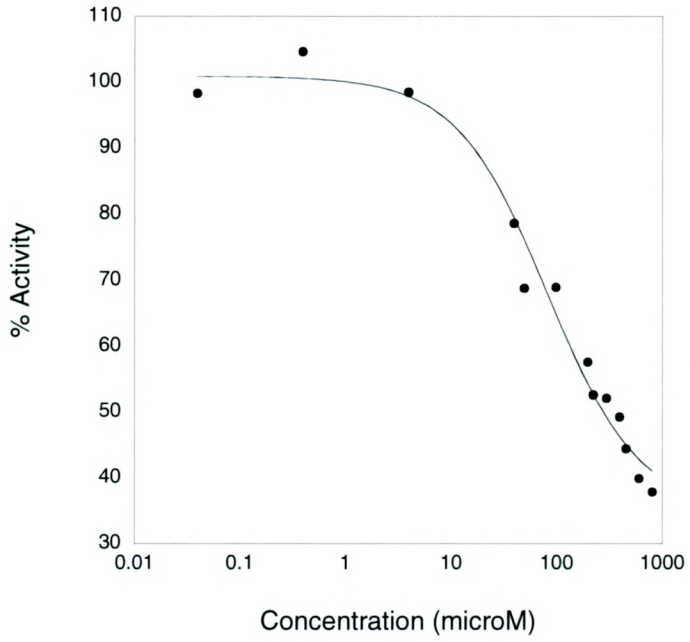

Figure 15. A representative graph of one of three separate trials of a *B. malayi* DHFR inhibition experiment carried out in the presence of the inhibitor Pyrimethamine. Data fit using KaleidaGraph. Individual experiments were conducted in a 96-well plate at room temperature with conditions in the well of 100 μM NAPDH, 100 μM DHF and 46 nM *Bm*DHFR. The average of the three trials gave an IC50 of 90.2 ± 7.9μM. Percent activity in the y-axis was determined by dividing the slope of the abs. of pyrimethamine at different concentrations vs. time over the slope of the assay (abs. vs. time) with no inhibitor, and multiplying by 100%.

PMT	IC50 (μM)	K_I (μM)
Trial 1	98.354	41.66581556
Trial 2	82.497	34.94829683
Trial 3	147.38	62.43475504
Average	109.4103333	46.34962248
Std. dev.	33.82503219	14.3293364
Average ± Std. dev.	109 ± 34	46 ± 14

Table 4. IC50 and K_I from three trials of Pyrimethamine.

3.6.3. Trimethoprim

Inhibition curve, IC50 and K_I determination:

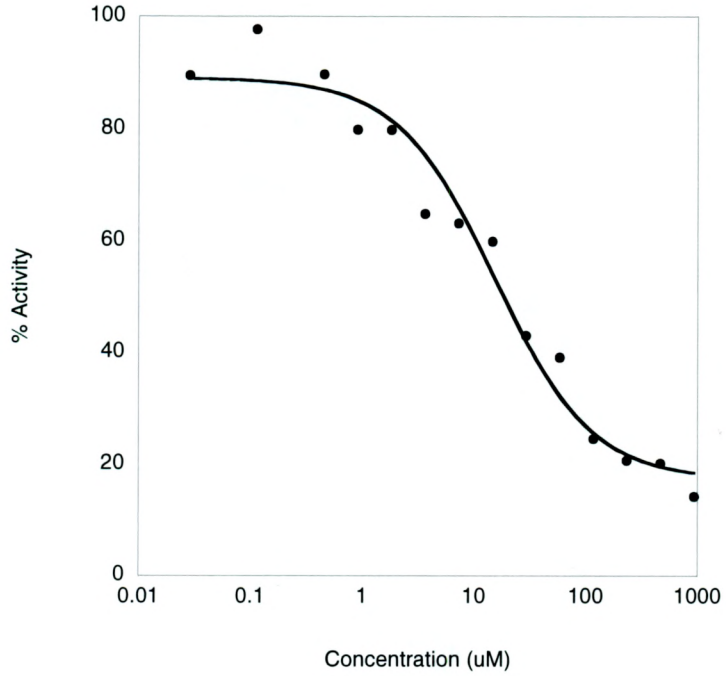

Figure 16. A representative graph of a *B. malayi* DHFR inhibition curve established in the presence of the inhibitor Trimethoprim. Data fit using KaleidaGraph. The average of three trials gave an IC50 of 31.8 ± 5.4μM. Individual experiments were conducted in a 96-well plate at room temperature with conditions in the well of 100 μM NAPDH, 100 μM DHF and 46 nM *Bm*DHFR. Percent activity in the y-axis was determined by dividing the slope of the abs. of trimethoprim at different concentrations vs. time over the slope of the assay (abs. vs. time) with no inhibitor, and multiplying by 100%.

TMP	IC50 (μM)	K_I (μM)
Trial 1	15.44	6.541
Trial 2	22.65	9.595
Trial 3	57.32	24.28
Average	31.80333333	13.472
Std. dev.	22.39020396	9.483742774
Average ± Std. dev.	32 ± 22	13 ± 9

Table 5. IC50 and K_I from three trials of Trimethoprim.

3.6.4. Cycloguanil

Inhibition curve, IC50 and K_I determination:

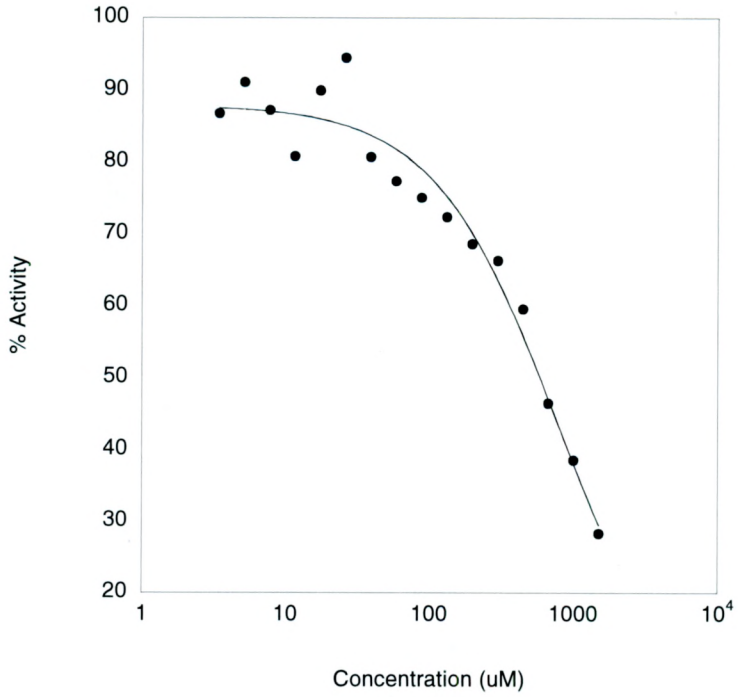

Figure 17. A representative graph of a *B. malayi* DHFR inhibition curve established in the presence of the inhibitor Cycloguanil. Data fit using KaleidaGraph. The average of three trials gave an IC50 of 770.6 ± 534μM. Individual experiments were conducted in a 96-well plate at room temperature with conditions in the well of 100 μM NAPDH, 100 μM DHF and 46 nM *Bm*DHFR. Percent activity in the y-axis was determined by dividing the slope of the abs. of cycloguanil at different concentrations vs. time over the slope of the assay (abs. vs. time) with no inhibitor, and multiplying by 100%.

CYC	IC50 (μM)	K_I (μM)
Trial 1	719.44	428.1687449
Trial 2	796.99	474.3219838
Trial 3	795.42	473.3876113
Average	770.6166667	458.6261134
Std. dev.	44.32724482	26.38099186
Average ± Std. dev.	771 ± 44	459 ± 26

Table 6. IC50 and K_I from three trials of Cycloguanil.

3.6.5. 2,4-Diaminoquinazoline

Inhibition curve, IC50 and K_I determination:

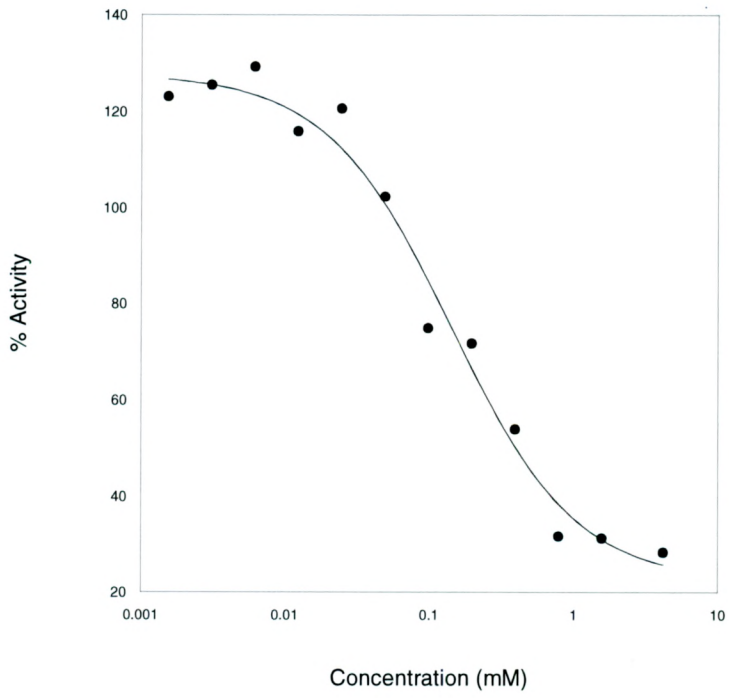

Figure 18. A representative graph of a *B. malayi* DHFR inhibition curve established in the presence of the inhibitor 2,4-Diaminoquinazoline. Data fit using KaleidaGraph. The average of three trials gave an IC50 of 192.9 ± 88.0μM. Individual experiments were conducted in a 96-well plate at room temperature with conditions in the well of 100 μM NAPDH, 100 μM DHF and 46 nM *Bm*DHFR. Percent activity in the y-axis was determined by dividing the slope of the abs. of 2,4-diaminoquinazoline at different concentrations vs. time over the slope of the assay (abs. vs. time) with no inhibitor, and multiplying by 100%.

2,4-Diaminoquinazoline	IC50 (μM)	K_I (μM)
Trial 1	137.89	58.41449568
Trial 2	117.72	49.86985591
Trial 3	205.66	87.12397695
Average	153.7566667	65.13610951
Std. dev.	46.06706235	19.5154414
Average ± Std. dev.	154 ± 46	65 ± 20

Table 7. IC50 and K_I from three trials of Cycloguanil.

3.7. Comparing experimental IC_{50} values in Table 8 for *B. malayi* DHFR to predictions

Compound	IC_{50} (μM)	K_I (μM)
Methotrexate	0.004 ± 0.0008	0.002 ± 0.0003
Pyrimethamine	109 ± 34	46 ± 14
Trimethoprim	32 ± 22	13 ± 9
Cycloguanil	771 ± 44	459 ± 26
2,4-Diaminopyrimidine	>20,000	>8,472
2,4-Diaminoquinazoline	154 ± 46	65 ± 20

Table 8. Summary of IC_{50} and K_i values for a set of antifolate compounds tested against *Bm*DHFR. Values are averages of at least triplicate experiments and standard deviations are shown. The experiments were conducted at pH 6.0, at room temperature, with 100 μM NADPH, 100 μM DHF, and 46 nM DHFR. The K_I values were obtained using the Cheng Prusoff equation (Prusoff 1973).

The predicted inhibitors' IC_{50} values from the literature are given in Table 1; they represent the values obtained for the DHFR homologs most similar to *B. malayi* DHFR in terms of the amino acid positions predicted to play a role in enzyme inhibition.[5] A comparison of the experimental to the expected values showed that the IC50's for methotrexate and trimethoprim were closest to the predictions. Methotrexate was confirmed to be the strongest inhibitor for *B. malayi* DHFR, this did not surprise because based on its close homology to *L. major* DHFR. However, IC50 values for other inhibitors like cycloguanil, pyrimethamine, and 2,4-diaminoquinazoline were not close to the predictions; they are considered weak inhibitors. They were expected to be better inhibitors based on the prediction from Table 1 showing that these compounds inhibit *L. major* with more potency. Notably, 2,4-diaminopyrimidine was determined not to be an inhibitor of *B. malayi* DHFR, despite the predictions and its similarity to 2,4-diaminoquinazoline. These findings suggest that perhaps a compound with a higher resemblance to the structure of 2,4-diaminoquinazoline could be a possible inhibitor for *B. malayi* DHFR. The extra ring in the 2,4-diaminoquinazoline structure could play a role in the inhibition of the DHFR enzyme. In conclusion, with varying potencies all compounds except for 2,4-diaminopyrimidine inhibited *Bm*DHFR, as it was expected.

3.8. Dissociation Constants for NADPH of Mutant and Wildtype *B. malayi* DHFR

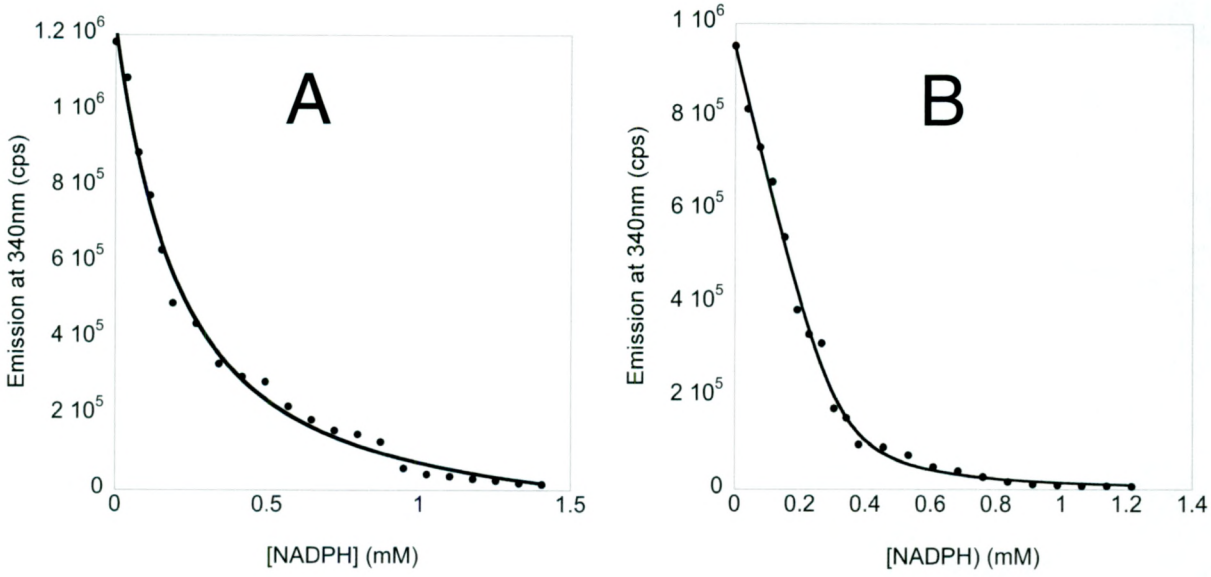

Figure 18. Dissociation constant (K_D) analysis of NADPH in the presence of the mutant (A) and wildtype (B) of *B. malayi* DHFR. Both graphs above are representative of three separate trials. Concentration of enzyme and NAPDH were ~200nM and 0 to 1.4 mM, respectively. The wavelength was at 340nm. The average for the mutant K_D was 129 ± 38 μM and the average for the wildtype K_D was 22 ± 14 μM.

Based on the K_D data we can conclude that $\Delta_{113\text{-}125}$*Bm*DHFR binds NADPH with a lower affinity than *Bm*DHFR. However, these findings suggest that the mutant enzyme is still able to fold to some extent. It can also be concluded that the 13 amino acids missing from the mutant enzyme are located on the βF-βG loop, by comparison with *E. coli* DHFR. In *E. coli* DHFR this loop plays a role in dynamics associated with catalysis, therefore we suggest that the βF-βG loop also plays the same role in *Bm*DHFR.

4. Summary

In summary, I expressed and purified the target enzyme, DHFR, in the *B. malayi* organism using a special strain of *E. coli* cells, LOBSTR, and an Ni-NTA affinity chromatography. The enzymatic characterization of *B. malayi* DHFR was carried out using the purified protein. The Michaelis-Menten constant, Km, was found to be 14.7 ± 3.6μM, which shows that the enzyme has high affinity for the substrate. The turnover number, k_{cat}, and the equilibrium dissociation constant, K_D, for NADPH was found to be 1.4 ± 0.1s^{-1} and 22 ±0.01μM, respectively. The inhibition studies showed that methotrexate was the strongest inhibitor. However, methotrexate is used for chemotherapy and is an immunosuppressant, a fact that makes it unsuitable for the treatment of lymphatic filariasis in human patients. Trimethoprim ranks second after methotrexate in IC50 and K_I value, suggesting that perhaps it can be a lead compound in the search for a more potent and less toxic drug. Obtaining the crystal structure of *Bm*DHFR in the presence and absence of a high affinity inhibitor is the obvious next step to be undertaken, in order for organic chemists to have a good understanding of the binding site of the enzyme and be able to work on optimizing existing compounds to fit in the active site while keeping toxicity and side effects to a minimum. The present project thus might serve as the basis for the discovery of a potent compound that will hopefully make it to the market to help cure this neglected disease that affects millions of unprivileged people.

5. Bibliography

1. Andersen, K. R.; Leska N. C.; Schwartz T. U. Optimized E. coli expression strain LOBSTR eliminates common contaminants from His-tag purification, *Proteins: Structure, Function, and Bioinformatics* **2013**, *81*, 1857-1861.

2. Bag, S.; Tawari, N. R.; Sharma, R.; Goswami, K., Reddy, M. V. R.; Degani M. S. *In vitro* biological evaluation of biguanides and dyhydrotriazines against *Brugia malayi* and folate reversal studies, *Acta Tropica* **2013**, *113*, 48-51.

3. Chan D. C; Anderson A. C. Towards species-specific antifolates, *Current Medicinal Chemistry* **2006**, *13*, 377-398

4. Gilbert, I. H. Inhibitors of dihydrofolate reductase in leishmanial and trypanosomes, *Biochimica et Biophysica Acta* **2002**, *1587*, 249-257.

5. Goodey, N. M., et al. (2011) Prediction of residues involved in inhibitor specificity in the dihydrofolate reductase family, *Biochimica et Biophysica Acta (BBA)-Proteins and Proteomics* **2011**, *1814*, 1870-1879.

6. Hammes-Schiffer S. Hydrogen tunneling and protein motion in enzyme reactions, *Acc. Chem. Res.* **2005,** *39*, 93-100.

7. Hande, S., et al. Targeting folate metabolism for therapeutic option: A bioinformatics approach, *Indian Journal of Experimental Biology* **2015**, *53,* 762-766.

8. Howell E. E.; Villafranca J. E.; Warren M. S.; Oatley S. J.; Kraut J. (1986) Functional role of aspartic acid-27 in dihydrofolate reductase revealed by mutagenesis, *Science 231*, 1123–28.

9. *KaleidaGraph,* version 4.1, *Synergy Software* 2002. (accessed 2015)

10. Khabnadideh, S., et al. Design, synthesis and evaluation of 2,4-diaminoquinazoline as inhibitors of trypanosomal and leishmanial dihydrofolate reductase, *Bioorganic & Medicinal Chemistry* **2005**, *13*, 2637-2649.

11. Liu, T., et al. BindingDB: a web-accessible database of experimentally determined protein–ligand binding affinities, *Nucleic acids research* **2007**, *35*, D198-D201.

12. Venkitakrishnan, R. P., et al. Conformational Changes in the Active Site Loops of Dihydrofolate Reductase during the Catalytic Cycle, *Biochemistry* **2004**, *43*, 16046-16055.

13. Pez, D., et al. 2,4-Diaminopyrimidines as Inhibitors of Leishmanial and Trypanosomal Dihydrofolate Reductase. *Bioorganic & Medicinal Chemistry* **2003**, *11*, 4693-4711.

14. Cheng Y.; Prusoff W. H. Relationship between the inhibition constant (K_I) and the concentration of inhibitor which causes 50 per cent inhibition (IC_{50}) of an enzymatic reaction, *Biochem. Pharmaco.* **1973**, *22*, 3099–3108.

15. Sharma, M.; Chauhan, P.M. Dihydrofolate reductase as a therapeutic target for infectious diseases: opportunities and challenges, *Future Med Chem* **2012**, *4*, 1335-65.

16. Sharma, R. D., et al. Exploration of 2,4-diaminopyrimidine and 2,4-diamino-*s*-triazine derivatives as potential antifilarial agents, *Parasitology FEMS Microbiology Letters* **2012**, *140*, 101-105.

17. UniProt Consortium, UniProt: a hub for protein information, *Nucleic acids research* **2015**, *43*, D204-D212.

18. White, E. L.; Ross, L. J.; Cunningham, A.; Escuyer, V. Cloning, expression, and characterization of *Mycobacterium tuberculosis* dihydrofolate reductase, *FEMS Microbiology Letters* **2004**, *232*, 101-105.

19. World Health Organization: Lymphatic filariasis. http://www.who.int/en/. (accessed 2016)